Numerical Analysis of Anode Sheath Structure Transition in an Anode-layer Type Hall Thruster

Shigeru Yokota[1] ,Kimiya Komurasaki[2], and Yoshihiro Arakawa.[3]
The University of Tokyo, Tokyo, 113-8656, Japan

Electrical sheath structure and plasma dynamics inside a hollow anode are numerically computed using a fully kinetic 2D3V Particle-in-Cell (PIC) / Direct Simulation Monte Carlo (DSMC) code. By treating electrons and ions as particles, temporal and spatial variations of the non-neutral plasma near the anode surface were analyzed. The code was verified in terms of the neutral decay time and discharge current waveform. The simulation results show that in the stable region, which corresponds to the low magnetic flux density case, electrons penetrated deeply into the anode hollow. Then, an ion sheath is created on the anode surface due to the high ionization rate in the hollow. The propellant utilization by the anode exit is estimated at 45%. In the "ionization oscillation" region, which corresponds to the high magnetic flux density case, an ion sheath and electron sheath appeared alternately. An electron sheath was formed in the vicinity of the anode surface because of the lack of electron density for sustaining discharge.

Nomenclature

B	=	magnetic flux density
D	=	anode hollow width
e	=	electric charge
E	=	electric field strength
I_d	=	discharge current
m	=	particle mass
n	=	number density
t	=	time
V_d	=	discharge voltage
Z	=	distance between anode tip and channel exit
ε_0	=	free space permeability
ϕ	=	space potential
ν	=	collision frequency
r, z, θ	=	cylindrical coordinate

I. Introduction

Ionization oscillation in anode layer hall thrusters would be one of the serious problems to be overcome. A hollow anode is commonly used to stabilize the discharge for these thrusters.[1-3)] However, the mechanism of discharge stabilization using a hollow anode is still unknown and optimization of anode design has not been done.

The goal of our study is to model the sheath structure on the electrode, which has a great effect on the stable discharge of anode layer hall thrusters, and to find out optimum anode design. However, it would be very difficult to measure plasma potential and density inside a hollow anode because plasma density is expected very small and the plasma is electrically non-neutral.

In this study, the structure of electrical sheath inside a hollow anode was numerically simulated using the fully kinetic 2D3V Particle-in-Cell (PIC) and Direct Simulation Monte Carlo (DSMC) methodologies.[4-8)] The results are compared with the measurement using a 1-kW class anode layer hall thruster.

[1] Graduate student, Department of Aeronautics and Astronautics, yokota@al.t.u-tokyo.ac.jp
[2] Associate Professor, Department of Advanced Energy, komurasaki@k.u-tokyo.ac.jp
[3] Professor, Department of Aeronautics and Astronautics, arakawa@al.t.u-tokyo.ac.jp

II. Discharge Current Oscillation

The University of Tokyo anode layer hall thruster has a hollow anode as shown in Fig. 1. It has two guard rings made of stainless steel kept at the cathode potential. The inner and outer diameters of the rings are 48mm and 62mm, respectively. Magnetic flux density is variable by changing the current of a solenoid coil set at the center of the thruster[3,4]. Xenon is used as a propellant.

A photograph of the hollow anode is shown in Fig. 2. It has an annular hollow anode made of cupper. *Z* denotes

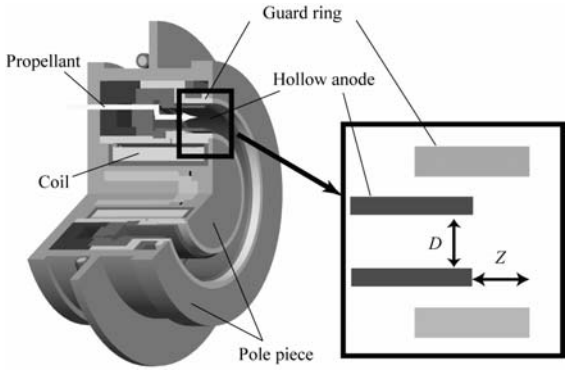

Figure 1. The University of Tokyo Anode Layer Hall Thruster.

Figure 2. A hollow anode and an acceleration channel.

the distance between the channel exit and the anode tip, and *D* does the width of anode hollow.

Figure 3 shows measured oscillation amplitude Δ of the discharge current for *Z*=1~4mm and *D*=1~3mm. The amplitude was defined as,

$$\Delta = \sqrt{\int_0^\tau (I_d - \overline{I}_d)^2 dt \Big/ \tau} \tag{1}$$

The oscillation amplitude was sensitive to the magnetic flux density *B* and threshold for stable discharge was about 11-15mT. Figure 4 shows the time-averaged discharge current $\overline{I_d}$ and *B* for a certain operation condition. Although the oscillation is small at *B*<14mT, the thrust efficiency is poor because of large electron backflow current in this range of *B*. Therefore, the desirable operation condition is limited in a quite narrow range of *B*.

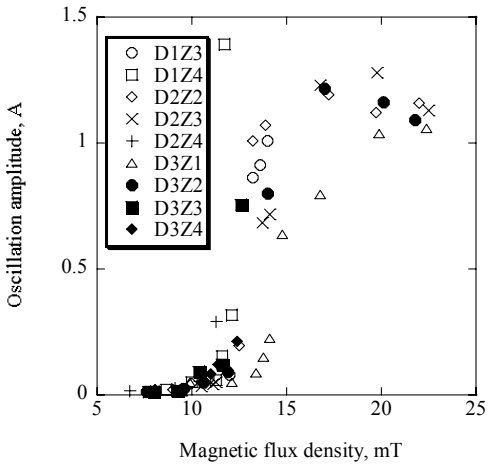

Figure 3. Oscillation amplitude. *propellant flow rate 1.0A$_{eq}$=1.37mg/s, discharge voltage 400V*

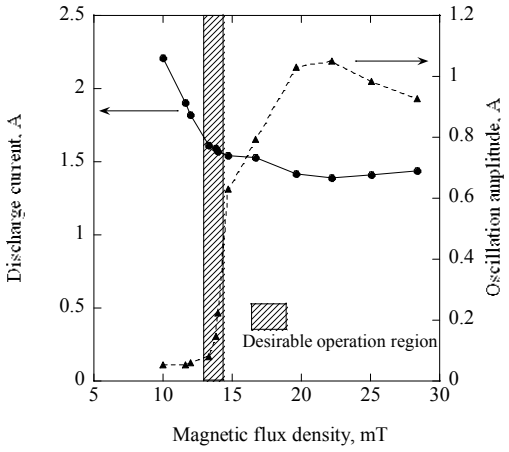

Figure 4. Averaged discharge current and oscillation amplitude. *mass flow rate 1.0A$_{eq}$=1.37mg/s, discharge voltage 250V.*

III. Computation Method

A. Computational models and assumptions

Both electrons and ions are treated as a particle. In the code, 10^6-10^9 of real particles are regarded as one macro-particle and treated kinetically. Only singly charged ionization is considered and mass ratio m_e/m_n is decreased from 4×10^{-6} to 1/100, to speed up the calculation.

Figure 5 shows the flow chart of calculation. Electric and magnetic forces are implemented via the PIC method and collisions are via the DSMC method. The plasma potential ϕ is calculated using the Poisson's equation as,

$$\frac{\partial^2\phi}{\partial z^2}+\frac{1}{r}\frac{\partial}{\partial r}\left(r\frac{\partial\phi}{\partial r}\right)=-\frac{e}{\varepsilon_0}(n_i-n_e) \tag{2}$$

Here, r, and z are the cylindrical coordinates and n_i, n_e, e, ε_0 are the ion and electron number density, electronic charge and electric permeability, respectively.

The three highest frequency collisions; Xe - e^- ionization collision, Xe - e^- excitation collision and e^- - e^- elastic scattering are considered. In addition, the Bohm diffusion coefficient is implemented in terms of the virtual collision frequency as

$$\nu_{\text{Bohm}}=\frac{1}{16}\frac{eB}{m_e}. \tag{3}$$

Total collision frequency is defined as

$$\nu_{\text{total}}=\nu_{\text{elastic}}+\nu_{\text{ionization}}+\nu_{\text{excitation}}+\nu_{\text{Bohm}}. \tag{4}$$

The simulation time step is set typically at 1.22×10^{-11}s based on the Larmor frequency that is one order of magnitude larger than the total collision frequency.

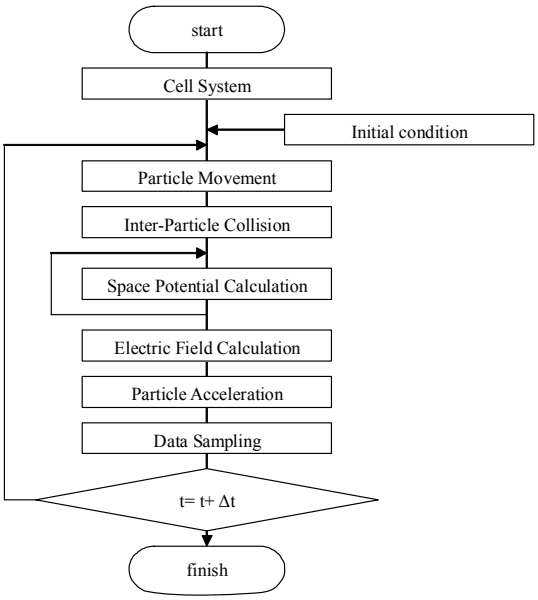

Figure 5. Calculation flow chart.

B. Computational grid and boundary conditions

The cylindrical coordinate system (r, z, θ) was used as shown in Fig. 6. Particle's position is expressed in two-dimensional space r and z, while its velocity is expressed in three-dimensional space. That is, particles move in all directions, but the azimuthal coordinate is always discarded.

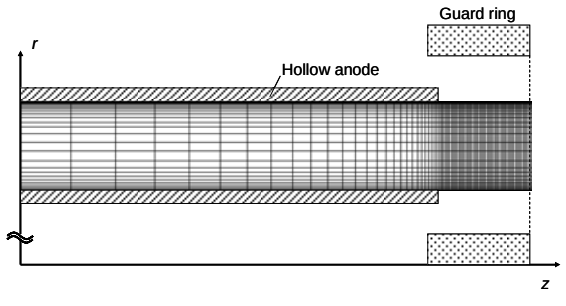

Figure 6 The coordinate system and computational grid.

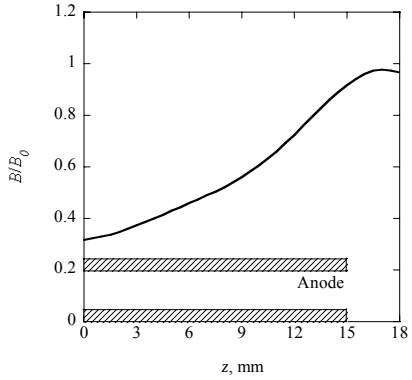

Figure 7. Magnetic flux density distribution assumed in this simulation.

An orthogonal computational grid is used. In order to observe the sharp density variation in the vicinity of anode exit, the axial cell length is getting smaller toward the anode while the radial cell length is getting smaller toward the anode surface. The minimum cell length is in the order of the Debye length.

Figure 7 shows the magnetic flux density distribution used in the calculation, which is identical to the actual distribution in the thruster. [4] The magnetic flux $2\pi rB(r)$ is constant. B_0 is variable.

Neutral particles are fed from the base of the anode hollow and assumed to be reflected on the anode surface boundary. Electrons are fed from the channel exit boundary with a T_e=10eV half-Maxwellian velocity distribution. The proper amount of electrons comes into the calculation region automatically by the neutral-electron collision. They reflect on the guard ring boundary, and lost on the anode surface boundary. Ions are produced only by ionization collisions in the computational domain, and lost on every boundary. Ions recombined with electrons on the anode surface return to the channel as neutral particles.

In solving the Poisson's equation, the Dirichlet condition was given on the anode surface and channel exit boundaries and the Neumann condition on the other boundaries.

C. Parallelization

This calculation code was parallelized using Message Passing Interface (MPI) because this code cost long time until calculation reached to the semi-convergence and large memory to deal with many particles. The data division method for particles is applied to the code, that is, the parts to calculate particles' movements, acceleration, and collision were parallelized, while the other parts were not because the particle calculation parts are most time and memory consuming. Concretely, the amount of neutral particles and electrons were divided by the processing elements equally. Before the field calculation, processing elements communicate with each other in order to obtain the total electron number density of each cell.

IV. Code Verification and Validation

A. Ionization rate

The ionization collision is the most important part of this code. The DSMC result was compared with the deterministic solution. Uniform mixture of electrons and neutral particle in unit volume is assumed. The conservation equations of particles and electron energy ε_e are expressed as

$$\frac{\mathrm{d}n_e}{\mathrm{d}t} = -\frac{\mathrm{d}n_n}{\mathrm{d}t} = n_n n_e \left\langle \sigma_{ion} \sqrt{2\varepsilon_e / n_e m_e} \right\rangle \tag{5}$$

$$\frac{1}{n_n n_e}\frac{\mathrm{d}\varepsilon_e}{\mathrm{d}t} = -\left\langle \sigma_{ion} \sqrt{2\varepsilon_e / n_e m_e} \right\rangle \varepsilon_{ion} - \left\langle \sigma_{exc} \sqrt{2\varepsilon_e / n_e m_e} \right\rangle \varepsilon_{exc} \tag{6}$$

respectively. Subscripts ion and exc denotes ionization collision and excitation collision, respectively. The result is shown in Fig.8.

Figure 9 shows the neutral decay time. It indicates that 200 electrons particles par a cell are necessary to correctly simulate the ionization collisions.

B. Discharge current

Figure 10 shows the computed average discharge current and oscillation amplitude. Although the computed discharge current is relatively smaller than measured current (see Fig. 4), the trend agrees well.

Figure 11 shows the discharge current histories in the case of B_0=20mT. The waveforms well resemble each other, as well as the oscillation frequencies. Both results indicate that the code is well reproducing the ionization oscillation in the anode- channel region.

C. Parallelization

Table 1 shows the CPU time of the each part during a time step in the case of 1 CPU and 8 CPU. The CPU time of particle calculation parts is reduced to a eighth. As a result, the total CPU time is reduced to a sixth. Figure 12 shows a discharge current history. The number of CPU does not affect on the calculation result.

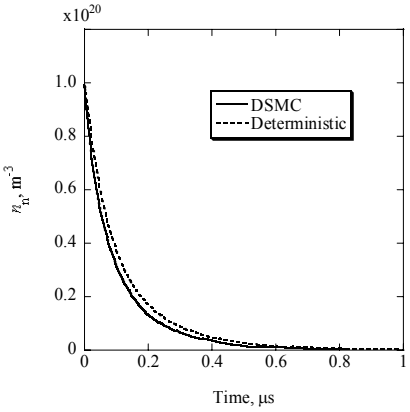

Figure 8. Comparison between the DSMC simulation and analytical solution.

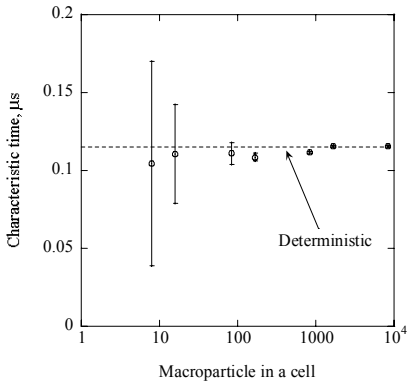

Figure 9. Neutral decay time vs. electron particle numbers per cell.

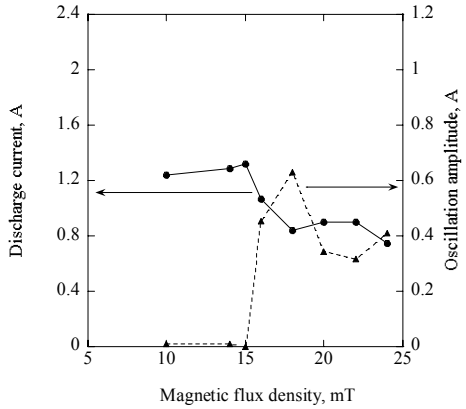

Figure 10.Computed discharge current and oscillation amplitude. *propellant flow rate $1.0A_{eq}$=1.37mg/s, discharge voltage 250V. D=3mm, Z=2mm.*

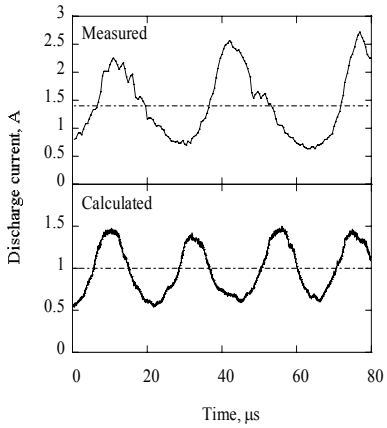

Figure 11.Compute and measured discharge current histories. *B_0=20mT.*

Table 1 CPU time during a time step

Part	Time, us	
	1CPU	8CPU
Particle movement	47.46094	13.24219
Inter particle collision	181.25000	22.38281
Message passing	0.07813	6.91406
Potential calculation	3.42855	3.45291
Field calculation	0.00000	0.00000
Particle acceleration	111.52344	14.45313
Total	343.74105	60.44510

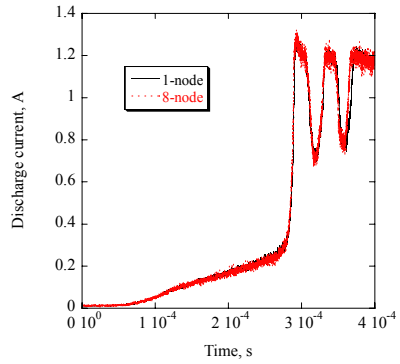

Figure 12. Discharge current history

V. Result and Discussions

A. In low *B* case

In the case of *B* lower than threshold magnetic flux density, electrons have a high mobility and easily penetrate into the anode hollow. As shown in Fig. 13, a high-electron-density region exists in the anode hollow. Thereby, ionization occurs mainly there.

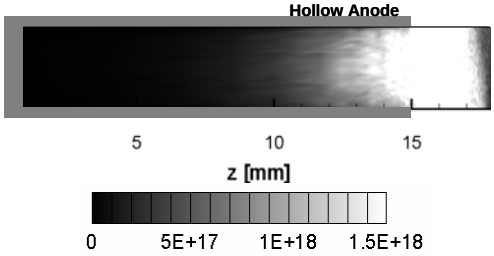

Figure 13. A 2-D distribution of the electron number density, B_0=15mT

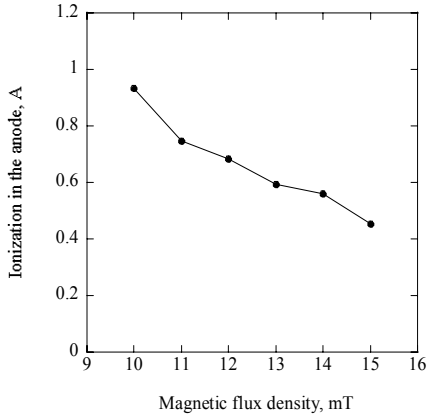

Figure 14. Relation between ion-production current in the anode and the magnetic flux density: propellant flow rate 1.0 Aeq.

Figure 14 shows the relation between the ion-production current in the hollow and applied *B*. The ionization region was swept downstream with *B*, and the ion production current was decreased to 0.45 A in the case of B_0=15mT, the right before the threshold. Figure 15 shows the 2-D plasma potential distribution. Potential is higher than anode potential in the hollow anode, and no sharp potential drop was observed at the anode exit. Figure 16 shows the 1-D potential distribution on the anode exit plane. (See Fig. 14) An ion sheath is formed on the anode surface. However, the sheath drop came to small value with *B* and vanished in the right before the threshold.

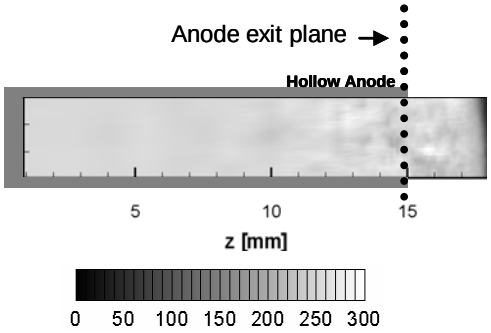

Figure 15. A 2-D distributions of plasma potential, B_0=15mT

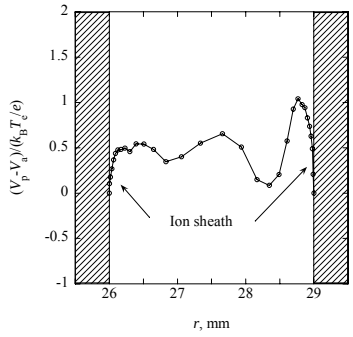

Figure 16. Plasma potential distribution on the anode exit plane, *The difference from the anode potential was normalized by the electron temperature on the middle hollow*

B. In high *B* case

When the applied magnetic flux density is higher than the threshold, ionization oscillation occurs. Figure 17 shows the history of the discharge current and the ion-production current in the hollow in the case of 16mT, which is right back of the threshold. The average ion-production current is as small as 0.35A.

The potential fluctuated and an ion sheath and an electron sheath appeared alternately on the anode surface. Figures 18 and 19 shows the 2-D plasma potential distribution and the 1-D distribution on the anode exit plane at $t=t_c$(Fig.17). The electron sheath appeared for about 80% of the time. This is because of the lack of electron number density on the anode surface was for sustaining stable discharge.

This sheath structure is the same as that of typical anode layer hall thrusters without the hollow anode: The "ionization oscillation" is inevitably induced in an electron sheath on the anode surface.

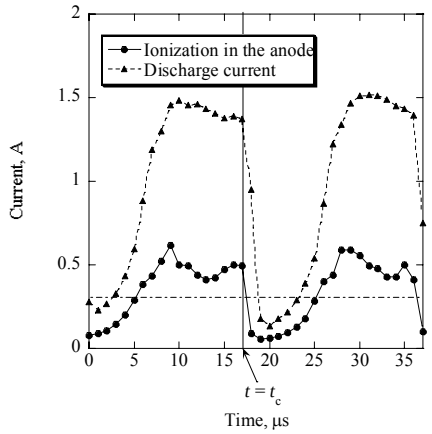

Figure 17. The correlation between the ion-production current in the hollow and discharge current, B_0=16mT.

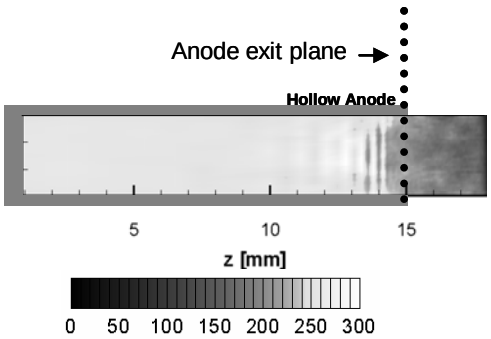

Figure 18. A 2-D plasma potential distribution, B_0=16mT.

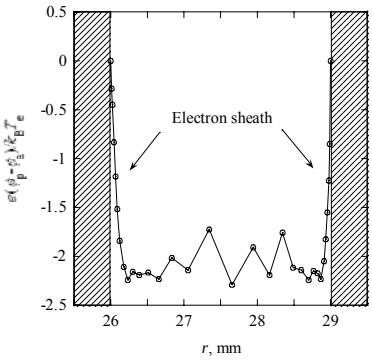

Figure 19. Plasma potential distribution on the hollow exit plane, B_0=16mT, $t=t_c$.

VI. Conclusion

A fully kinetic PIC-DSMC code successfully reproduced both stable and ionization oscillation modes observed in the experiment.

In the stable mode, this corresponds to the low magnetic flux density case, electrons penetrated deeply into the anode hollow. An ion sheath is created on the anode surface due to the high ionization rate in the hollow. The ion-production current in the hollow was decreased with the magnetic flux density from 0.95 A to 0.45A (from 95 to 45 % of the propellant flow rate). Thereby the sheath drop came to small value with *B* and vanished in the right before the threshold.

In the ionization oscillation mode, which corresponds to the high magnetic flux density case, ion-production current was decreased as small as 0.35 A at the right back of the threshold. The electron sheath was formed because of the lack of electron density on the anode surface This electron sheath would be the cause of the "ionization oscillation."

Acknowledgments

The present work was supported by a Grand-in-Aid for Scientific Research (S), No.16106012 sponsored by the Ministry of Education, Culture, Sports, Science and Technology in Japan.

References

[1]Semenkin A.V., Tverdokhlebov S.O., Garkusha V.I., Kochergin A.V., Chislov G.O., Shumkin B.V., Solodukhin A.V., Zakharenkov L.E., "Operating Envelopes of Thrusters with Anode Layer", IEPC2001-013, 27th International Electric Propulsion Conference, Pasadena, USA, October 2001.

[2]Semenkin, A., Kochergin, A., Garkusha, V., Chislov, G., Rusakov, A., "RHETT/EPDM Flight Anode Layer Thruster Development", IEPC-97-106, 25th International Electric Propulsion Conference, Cleveland, USA, August 1997.

[3]Yamamoto, N., Nakagawa, T., Komurasaki, K., Arakawa, Y., "Effect of Discharge Oscillations on Hall Thruster Performance", ISTS 2002-b-17, 23rd the International Symposium on Space Technology and Science, Shimane, Japan, May 2002.

[4]Yasui, S., Yamamoto, N., Komurasaki, K., Arakawa, Y., "Effect of Sheath Structure on Operating Stability in an Anode Layer Thruster," Proceedings of Asian Joint Conferences in Propulsion and Power 2004, pp.382-387, Seoul, Korea, March 2004.

[5]Hirakawa, M., "Particle Simulation of Plasma Phenomena in Hall Thrusters", IEPC-95-164, 24th International Electric Propulsion Conference, Moscow, Russia, September 1995

[6]Szabo, J. J., "Fully Kinetic Hall Thruster Modeling of a Plasma Thruster", PhD Thesis, Massachusetts Institute of Technology, 2001

[7] Szabo, J., Rostler, P., "One and Two Dimensional Modeling of the BHT-1000", IEPC-02-231, 28th International Electric Propulsion Conference, Toulouse, France, March 2003.

[8] Kumakura, K., Yasui, S., Komurasaki K., Arakawa, Y., "Plasma Modeling of a Hollow Anode for an Anode Layer Type Hall Thruster" IEPC-02-086, 28th International Electric Propulsion Conference, Toulouse, France, March 2003.